

Third harmonic beam profile generated in atmospheric air using femtosecond laser pulses

F. Théberge^{a,*}, N. Aközbek^b, W. Liu^a, J.-F. Gravel^a, S.L. Chin^a

^a *Département de Physique, de Génie Physique et d'Optique and Centre d'Optique, Photonique et Laser, Université Laval, Que., Canada G1K 7P4*

^b *Time Domain Corporation, 7057 Old Madison Pike, Huntsville, AL 35806, USA*

Received 20 July 2004; received in revised form 12 October 2004; accepted 12 October 2004

Abstract

We present, both experimentally and theoretically, the results on third harmonic generation in air during the filamentation of a powerful femtosecond laser pulse. The third harmonic beam pattern shows a central spot on the propagation axis at lower pump energy and is then surrounded by bright third harmonic conical emission at higher pump energy. We argue that the combined action of self-focusing and plasma generation in air plays an important role for the on-axis and off-axis phase-matching conditions along the filament resulting in high conversion efficiency. The experimental results are in good qualitative agreement with numerical simulations.

© 2004 Elsevier B.V. All rights reserved.

PACS: 42.65.Ky; 42.65.Jx; 52.35.Mw

Keywords: Femtosecond laser; Third harmonic; Filamentation; Air

1. Introduction

High-harmonic generation in gases has stimulated a lot of research interest because of its promising method for achieving high intensity, short wavelength coherent light sources [1]. In particular, third-harmonic (TH) generated in air with

femtosecond laser pulses has shown conversion efficiency as high as 0.2% [2–4] and potential applications in lidar measurements using time-resolved broadband spectroscopy [5,6]. The propagation of high peak power femtosecond laser pulses in transparent matter induces long filaments [7] and refocusing [8,9] along the propagation of the laser pulses. The mechanism for femtosecond laser pulses propagating over long distances in optical media is the dynamic interplay between the Kerr self-focusing due to nonlinear intensity-dependent

* Corresponding author. Tel.: +141865621314482; fax: +14186562623.

E-mail address: frthe81@phy.ulaval.ca (F. Théberge).

refractive index and defocusing from low-density plasma induced by multiphoton ionization. The plasma generation balances the self-focusing effect and leads to a limited beam diameter as well as limited peak intensity along the femtosecond laser pulse propagation. This is known as intensity clamping [10,11]. The peak intensity during filamentation in air is clamped down to about 5×10^{13} W/cm² which is sufficient to generate higher harmonics [2,4,12–14].

It has been demonstrated that as the intensity of the fundamental pulse I_ω increases, the TH energy generated in air is proportional to $I_\omega^{4.2}$ for low pump intensity and to $I_\omega^{0.45}$ for higher pump intensity [13,14]. The spectrum of the TH shows red shift or blue shift with respect to the three fold increase in frequency of the fundamental spectrum as a function of the pump energy and focal length lens used [3,4]. Recently, theoretical and experimental results have demonstrated that during femtosecond laser-induced filamentation in air an ultrashort TH pulse is generated forming a two-colored filament [2]. This two-color filamentation effect is due to a nonlinear intensity-dependent phase-locking between the fundamental and the TH pulses which could extend the phase-matching condition over longer propagation distance.

The purpose of this study was to further investigate the behavior of TH generation in air during the propagation of intense femtosecond laser pulses. To this end we measured the TH beam profile and the TH conversion efficiency at different pump energies. The experimental data are analyzed together with results of numerical simulations using a spatiotemporal dynamics model of the propagation of both the fundamental and the TH pulses. We shall show below that the third harmonic generated in air is due to both on-axis and off-axis phase-matching conditions along the propagation of the laser pulses which lead to a TH beam profile taking the form of a ring structure surrounding a central spot [4,15].

2. Experimental setup

The experiments were conducted using a Ti:sapphire chirped-pulse amplification (CPA) laser

system, which generates femtosecond laser pulses with a central wavelength at 807 nm, a repetition rate of 1 kHz and a transform limited pulse duration of 39 fs (FWHM). The diameter of the elliptic beam mode at the $1/e^2$ level was $d_H = 8.0$ mm and $d_V = 6.3$ mm where d_H and d_V are horizontal and vertical diameters, respectively. Laser pulses with energies ranging from 20 μ J to 2.0 mJ were focused into air at ambient pressure using a 100 cm focal length lens (L1). The far-field beam profile of the third harmonic generated in air was measured using an intensified CCD camera (ICCD) (see Fig. 1(a)). Dielectric dichroic mirrors (D1) with high reflectivity within the spectral range from 240 to 290 nm at 0° incident angle and high transmission for visible and infrared light, as well as a bandpass filter (B1) centered at 266 nm with a 25 nm bandwidth (FWHM) were fixed in front of the ICCD to suppress the fundamental pulse and image the third harmonic beam profile onto the time-gated detector.

Beyond the filament, the energy of the TH pulse was measured using a second experimental setup shown in Fig. 1(b). The fundamental pulse and the generated TH pulses were collimated using a plano-convex lens (L2) and then separated by two successive gratings (G1) and the TH energy was measured by a calibrated photomultiplier tube (PMT). The use of bandpass filter was avoided to prevent saturable transmission of the bandpass

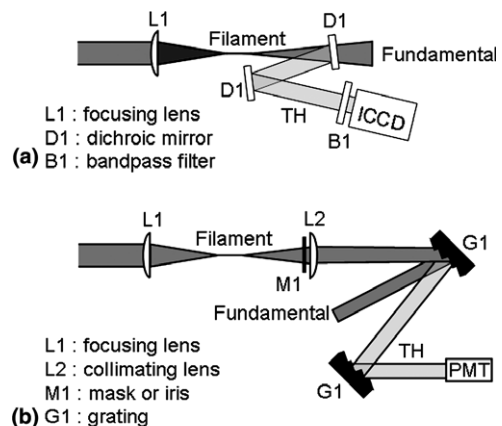


Fig. 1. Experimental setup for the (a) TH far-field beam profile imaging system and (b) TH energy measurement setup.

filter from high intensity of the fundamental pulse and third-harmonic pulse which could affect the energy measurement. In front of the collimating lens, an iris or a mask was installed to selectively transmit the TH central part or the TH ring structure, respectively, and their energy content was measured. The energy of the fundamental pulse was measured before the filament using a calibrated photodiode.

3. Experimental results

In order to study the TH generation in air, the characteristics of the third harmonic far-field beam profile and the energy of the TH as a function of the fundamental pulse energy are presented. In Fig. 2(a)–(d), the experimental results of the TH far-field beam profile generated in air using a 100 cm focal length lens are shown for four different

pump energies. We used the experimental setup described in Fig. 1(a) to investigate the fluence distribution of the TH. The relative intensity between the TH central spot and the rings were corrected for the transmission of the bandpass filter (central wavelength: 266 nm, bandwidth: 25 nm). The filter used in the experimental setup shown in Fig. 1(a) attenuated two times more the ring structure than the central spot due to different spectral composition in the ring part and the central spot of the TH beam profile (see below). For pump energy between 20 and 225 μJ (Fig. 2(a)), the spatial distribution of the TH emerging from the filament was limited to a rather smooth spot centered on the propagation axis and having half-angle divergence of 0.5 mrad. Starting from a pump energy of 225 μJ /pulse to 400 μJ /pulse, an interesting feature was observed: a ring appeared in the TH beam profile at a cone angle of 5 mrad surrounding the previous central spot (Fig. 2(b)). Using higher

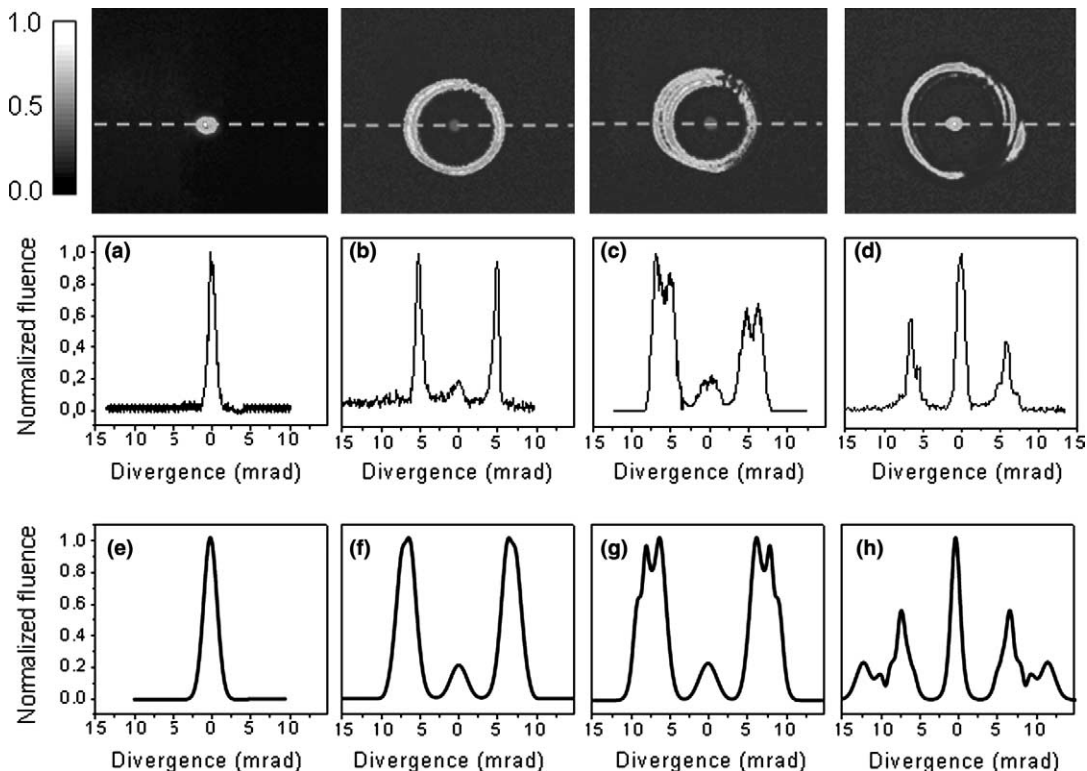


Fig. 2. TH pictures and profiles taken by ICCD camera at different pump energy (a) 100 μJ , (b) 400 μJ , (c) 500 μJ and (d) 1.3 mJ using 100 cm focal length lens. Simulated spatial profile of the TH at different pump energy (e) 85 μJ , (f) 340 μJ , (g) 510 μJ and (h) 1.278 mJ.

pump energy, the single ring observed in the TH beam profile changes to a set of complex ring structure shown in Fig. 2(c) and (d) at a cone angles between 5 and 6 mrad.

The experimental spectrum of the TH ring and central part are shown in Fig. 3 using a pump energy of 500 μJ . The spectral characteristics of each section of the third harmonic profile were measured with a spectrometer. The dash-dot line in Fig. 3 represents the cubic intensity distribution of the fundamental spectrum with a three fold increase in frequency (i.e. $F^3(3*\omega)$) measured after the filament. This spectrum is considered as a reference TH spectrum to show the relative red-shift and blue-shift of the TH spectral profile shown in Fig. 3. Using a 100 cm focal length lens and for the range of pump energies used in this experiment, the peak wavelength of the TH ring spectrum was centered around 273 nm, which is red-shifted relative to reference TH spectrum. The peak wavelength of the TH central part is measured to be around 267 nm, which is blue-shifted for the same range of pump energy. The FWHM spectral width of the TH ring is about 10 nm and the spectral width of the TH central part is around 3 nm.

Fig. 4(a) presents the total energy of the TH measured with a calibrated PMT and the energy contained in the TH central part and ring structure as a function of the input fundamental energy. For pump energies between 20 and 225 μJ , the total

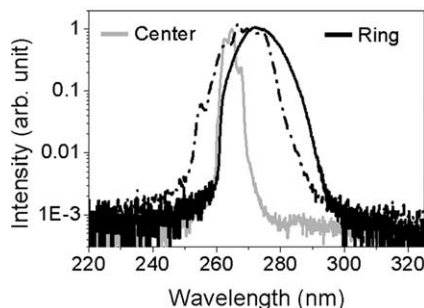


Fig. 3. Experimental TH spectrum of central part (gray line) and ring (black line) generated in atmospheric air at pump energy of 500 μJ using 100 cm focal length lens. The dash-dot line represents the cubic intensity of the fundamental spectrum with a three fold increase in frequency after the filament (i.e. $F^3(3*\omega)$).

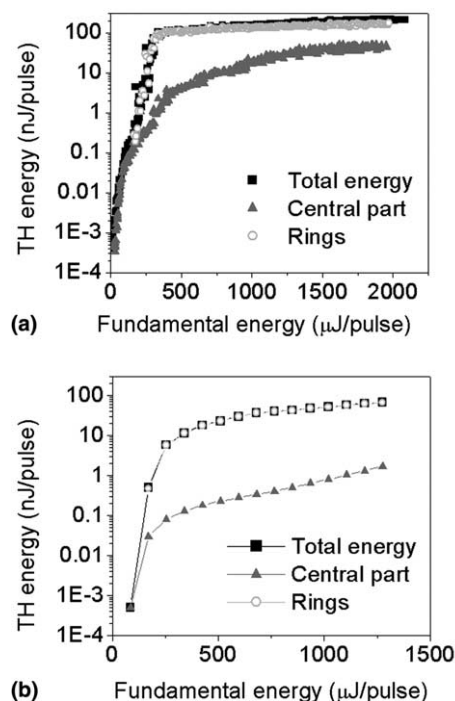


Fig. 4. Total energy of the TH generated in air as function of the fundamental energy and the TH energy contained in the rings structure and central spot using 100 cm focal length lens (a) experimental measurements done with setup shown in Fig. 1(b) and (b) numerical simulation.

energy of the TH is mainly due to the TH central part, which is well correlated with the recorded TH beam profile (see Fig. 2(a)). Power-law dependence with an exponent of 3.3 is observed for this range of energy for both the total energy and the energy contained in the central spot. However, for pump energies between 225 and 330 μJ , we observed a faster exponential growth of the total TH energy which is associated to a rapid increase of the TH ring energy. For this range of pump energies, most of the TH energy is contained in the rings structure and both the total TH energy and TH ring energy have a power-law exponent of 9. The steep change of the exponential growth in the TH ring energy as a function of the pump energy is observed to correspond to a pump pulse energy reaching the intensity clamping regime in atmospheric air. Using higher pump energy (between 330 μJ to 2 mJ), the energy of the TH rings structure

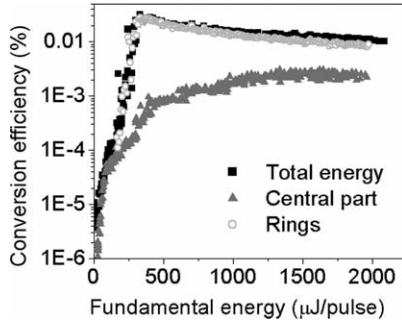


Fig. 5. Measured conversion efficiency of the TH generated in atmospheric air as function of the fundamental energy.

saturated and the TH central spot energy continued to increase but at a much slower rate; more than 90% of the total TH energy is contained in the rings structure.

Fig. 5 presents the experimental TH conversion efficiency (TH energy/pump energy) on the fundamental laser energy for 100 cm focal length lens. An interesting feature is that the total as well as the ring's conversion efficiency increases rapidly to a maximum and then decreases slowly with further increase of the fundamental energy. The maximum conversion efficiency corresponds to a pump energy at which the energy contained in the TH ring starts to saturate. The conversion efficiency of the TH central part increases with pump energy and becomes constant for pump energy higher than 1.5 mJ.

4. Numerical simulations

An important requirement for the efficient generation of harmonics is that the phase should be matched over an appreciable interaction length. In the limit of perfect phase matching, it is known that for a tightly focusing geometry there is no net TH generation since the light generated prior to the focus destructively interferes with the TH generated after the geometrical focus. This is the result of the Guoy phase shift in which the TH energy generated before the focus is given back to the pump [16]. As the intensity of the pump increases (or pump energy) nonlinear effects become important which changes the phase of the pump [17,18]

and starts to compensate for the Guoy shift where efficient TH can be generated [2]. Third harmonic generation in air from high-power femtosecond laser pulses includes effects such as diffraction, self-focusing, plasma generation and group-velocity dispersion. In this respect, a rigorous theoretical analysis of the full dynamics and interaction of both the pump and third-harmonic pulses is required. Our model is described by a set of coupled equations, which can be written in dimensionless form in the retarded coordinate system ($\tau = t - z/v_g(\omega)$) as:

$$\left(i \frac{\partial}{\partial z} + \frac{1}{4} \nabla_{\perp}^2 - i \frac{L_{DF}}{4L_d} \frac{\partial^2}{\partial \tau^2} + i \frac{L_{DF}}{L_{Abs}} |\varepsilon_{\omega}|^{2n-2} \right) \varepsilon_{\omega} + \frac{L_{DF}}{L_{NL}} \left(|\varepsilon_{\omega}|^2 \varepsilon_{\omega} + \varepsilon_{\omega}^{*2} \varepsilon_{3\omega} + 2 |\varepsilon_{3\omega}|^2 \varepsilon_{\omega} \right) - \frac{L_{DF}}{L_{PL}} N_e \varepsilon_{\omega} = 0, \quad (1)$$

$$\left(i \frac{\partial}{\partial z} + \frac{1}{12} \nabla_{\perp}^2 + i \frac{L_{DF}}{L_{\Delta v}} \frac{\partial}{\partial \tau} - i \frac{L_{DF}}{4L'_d} \frac{\partial^2}{\partial \tau^2} + \frac{L_{DF}}{L_{\Delta k}} \right) \varepsilon_{3\omega} - \frac{L_{DF}}{3L_{PL}} N_e \varepsilon_{3\omega} + i \frac{L_{DF}}{L_{Abs}} |\varepsilon_{3\omega}|^{2n-2} \varepsilon_{3\omega} + \frac{3L_{DF}}{L_{NL}} \left(|\varepsilon_{3\omega}|^2 \varepsilon_{3\omega} + \frac{\varepsilon_{\omega}^3}{3} + 2 |\varepsilon_{\omega}|^2 \varepsilon_{3\omega} \right) = 0, \quad (2)$$

$$\frac{\partial N_e(\tau)}{\partial \tau} = (\Gamma_{\omega} + \Gamma_{3\omega}) [1 - N_e(\tau)]. \quad (3)$$

Here, ε_{ω} and $\varepsilon_{3\omega}$ are the electric field envelope functions, normalized to the peak value of the input pump field $\varepsilon_0 = \sqrt{2P_0/\pi w_0^2}$. The subscripts ω and 3ω denote the fundamental and TH pulses, respectively. The propagation direction z is given in units of $L_{DF} = k_{\omega} w_0^2/2$, the temporal coordinate τ in units of the input pulse width τ_0 , and the transverse coordinate r in units of the input beam radius w_0 . The following length scales are also used: $L_{NL} = (n_2 k_{\omega} I_0)^{-1}$ is a nonlinear length scale, where $I_0 = |\varepsilon_0|^2$, n_2 is the nonlinear index of refraction, and $L_{PL} = k_{\omega} m_e c^2 / 2\pi e^2 N_0$ is the plasma length scale, where N_0 is the number density of neutral air molecules. $L_{\Delta v} = [v_g^{-1}(3\omega) - v_g^{-1}(\omega)]^{-1} \tau_0$, represents the characteristic temporal walk-off distance due to the group-velocity mismatch between the

two pulses, where $v_g(\omega)$ and $v_g(3\omega)$ are the group velocities of the pump and TH pulses, respectively. $L_d = \tau_0^2/2k''_\omega$ and $L'_d = \tau_0^2/2k''_{3\omega}$ are the length scales due to group-velocity dispersion of the fundamental and third harmonic, respectively, where $k''_\omega = 0.2 \text{ fs}^2/\text{cm}$ and $k''_{3\omega} = 1.0 \text{ fs}^2/\text{cm}$. Finally, $L_{\Delta k} = |\Delta k|^{-1} = |3k_\omega - k_{3\omega}|^{-1}$ is the linear wave vector mismatch length scale in the wave vectors $k_\omega = n_\omega k_0$ and $k_{3\omega} = n_{3\omega} 3k_0$, where $\Delta k = 3k_0(n_\omega - n_{3\omega}) = -5.0 \text{ cm}^{-1}$. Electron generation through multiphoton ionization of N_2 and O_2 is taken into account by the rates Γ_ω and $\Gamma_{3\omega}$, which are approximated by fitting the ionization rates into the form σI^n for the relevant intensity range, using the model of Muth-B  hm et al. [19]. The electron density N_e is normalized to N_0 , and $L_{\text{Abs}} = N_0 \sigma / 2n\hbar\omega$ accounts for ionization losses.

For the numerical simulations we have considered the propagation of a linearly polarized, collimated Gaussian input laser pulse with a center wavelength at $\lambda_0 = 807 \text{ nm}$ and a pulse duration $\tau_{\text{FWHM}} = 40 \text{ fs}$; this is then focused with a lens of focal length of 100 cm in air at atmospheric pressure. We verified the numerical results by changing the value of the critical power of self-focusing and beam radius. It appears that TH energy and far field pattern are dependent on these parameters. The qualitative results such as the central part and the ring structure remain the same, but they appear at different pump energies in the simulations than in the experiments. We have used laser input powers, P_0 , below and above the critical power, $P_{\text{cr}} = \lambda_0^2/2\pi n_\omega n_2 = 10 \text{ GW}$ needed for self-focusing in air. The initial transverse beam profile in the experiment was more elliptic. However, the numerical code is limited to a cylindrical symmetric beam profile and we therefore chose an effective initial beam radius of $w_0 = 3 \text{ mm}$ (at $1/e^2$ of intensity) for the numerical simulations. The set of Eqs. (1)–(3) were then integrated numerically with the initial condition $\varepsilon_{3\omega}(z=0) = 0$.

The numerical results for the far-field TH fluence distribution at 20 cm beyond the geometrical focus are shown in Fig. 2(e)–(h). For pump powers below the critical power for self-focusing, the TH generation is limited to a central spot (Fig. 2(e)) and the TH conversion efficiency is low (see Fig. 4(b)). As the pump energy is further increased

the nonlinear phase compensates the Guoy phase shift on-axis but there is a preferable phase-matching achieved off-axis since the beam has a cone of available wave vectors. For pump powers around the critical power for self-focusing in air, a TH ring appeared at a cone angle of 6 mrad and a significant on-axis component of the TH is still observed (see Fig. 2(f)). The simulated cone angle ($\theta = 6 \text{ mrad}$) and the relative fluence distribution between the ring and the central part are almost equal to the value measured from the above experimental results. However in this regime, Fig. 4 shows that on-axis TH is generated but not as efficiently as off-axis and the energy in the TH central part and rings start to deviate from each other. For pump energies higher than $350 \text{ }\mu\text{J}$, the intensity along the filament is clamped and a longer filament is generated. In the latter case, we may expect that as the filament length is increased more energy should be converted to the TH. However, along the propagation of the filament a slight spatial walk-off between the pump and TH conical emission is created and limits the efficient TH generation at the expected cone angle. This suggests that most of the TH ring energy is generated at the beginning of the self-focusing distance. If the pump energy is increased above the threshold for self-focusing and the length of the filament is increased, the TH ring energy saturated and the single ring obtained in the TH beam profile changed to a complex ring structure (Fig. 2(g) and (h)). This multiple rings structure is due to multiple phase-matching condition achieved off-axis at different cone angles as the pump energy is increased [17,18,20].

However, for pump energies above the threshold for self-focusing, the on-axis TH is still efficiently generated as the pump energy is increased despite the fact the peak pump intensity does not significantly increase anymore after $400 \text{ }\mu\text{J}$. Then, there must be some quasi-phase matching achieved on-axis so that as the interaction length is increased, more energy is converted to the TH central part (see Fig. 2(h)) which catches up as the pump energy is increased (see Fig. 4(b)). This phase-matching condition of the central part on longer propagating distance is due to a nonlinear intensity-dependent phase-locking between

the fundamental pulse and the TH central part [2].

5. Summary and conclusions

In conclusion, we have shown that third-order harmonic generation in air by high power near-infrared femtosecond laser pulses results in both on-axis and off-axis phase-matching conditions. The third-harmonic conical emission appeared at pump power around the critical power for self-focusing where off-axis phase-matching conditions have been generated at the beginning of the filament. The TH rings energy increased rapidly with strong conversion efficiency and then saturated for higher pump energy. On-axis TH increased exponentially with pump power below and above the critical power of self-focusing. The central part of the TH beam profile was phase-matched with the pump pulse over longer propagation distances due to the nonlinear intensity-dependent phase-locking. However, for the range of pump energies considered in this paper, most of the TH energy generated in air was attributed to conical emission.

Acknowledgements

This work was supported by Natural Sciences and Engineering Research Council of Canada (NSERC), Le Fonds Qu  b  cois de la Recherche sur la Nature et les Technologies (FQRNT), Canada Research Chairs (CRC), Canada Foundation for Innovation (CFI) and Canadian Institute for Photonic Innovations (CIPI). The authors appreciate the technical support of Mr. Mario Martin.

References

- [1] H.T. Kim, I.J. Kim, V. Tosa, Y.S. Lee, C.H. Nam, *Appl. Phys. B* 78 (2004) 863.
- [2] N. Ak  zbek, A. Iwasaki, A. Becker, M. Scalora, S.L. Chin, C.M. Bowden, *Phys. Rev. Lett.* 89 (2002) 143901.
- [3] H. Yang, J. Zhang, J. Zhang, L.Z. Zhao, Y.J. Li, H. Teng, Y.T. Li, Z.H. Wang, Z.L. Chen, Z.Y. Wei, J.X. Ma, W. Yu, Z.M. Sheng, *Phys. Rev. E* 67 (2003) 015401.
- [4] J. Peatross, S. Backus, J. Zhou, M.M. Murnane, H.C. Kapteyn, *J. Opt. Soc. Am. B* 15 (1998) 186.
- [5] N. Ak  zbek, A. Becker, M. Scalora, S.L. Chin, C.M. Bowden, *Appl. Phys. B* 77 (2003) 177.
- [6] P. Rairoux, H. Schillinger, S. Niedermeier, M. Rodriguez, F. Ronneberger, R. Sauerbrey, B. Stein, D. Waite, C. Wedekind, H. Wille, L. W  ste, C. Ziener, *Appl. Phys. B* 71 (2000) 573.
- [7] H. Schroeder, S.L. Chin, *Opt. Commun.* 234 (2004) 399.
- [8] W. Liu, S.L. Chin, O. Kosareva, I.S. Golubtsov, V.P. Kandidov, *Opt. Commun.* 225 (2003) 193.
- [9] K.D. Moll, A.L. Gaeta, *Opt. Lett.* 29 (2004) 995.
- [10] A. Becker, N. Ak  zbek, K. Vijayalakshmi, E. Oral, C.M. Bowden, S.L. Chin, *Appl. Phys. B* 73 (2001) 287.
- [11] W. Liu, S. Petit, A. Becker, N. Ak  zbek, C.M. Bowden, S.L. Chin, *Opt. Commun.* 202 (2002) 189.
- [12] S. Backus, J. Peatross, Z. Zeek, A. Rundquist, G. Taft, M.M. Murnane, H.C. Kapteyn, *Opt. Lett.* 21 (1996) 665.
- [13] A.B. Fedotov, N.I. Koroteev, M.M.T. Loy, X. Xiao, A.M. Zheltikov, *Opt. Commun.* 133 (1997) 587.
- [14] C.-J. Zhu, Y.-D. Qin, H. Yang, S.-F. Wang, Q.-H. Gong, *Chin. Phys. Lett.* 18 (2001) 57.
- [15] B. Eberle, H. B  rsing, D. Seiffer, R. Sauerbrey (personal communication).
- [16] R.W. Boyd, *J. Opt. Soc. Am.* 70 (1980) 877.
- [17] N. Ak  zbek, C.M. Bowden, S.L. Chin, *J. Mod. Opt.* 49 (2002) 475.
- [18] N. Ak  zbek, M. Scalora, C.M. Bowden, S.L. Chin, *Opt. Commun.* 191 (2001) 353.
- [19] J. Muth-B  hm, A. Becker, F.H.M. Faisal, *Phys. Rev. Lett.* 85 (2000) 2280.
- [20] S.L. Chin, S. Petit, W. Liu, A. Iwasaki, M.-C. Nadeau, V.P. Kandidov, O.G. Kosareva, K.Y. Andrianov, *Opt. Commun.* 210 (2002) 329.